

Cite this: *Dalton Trans.*, 2022, **51**, 1216

2-(4-Hydroxyphenyl)benzothiazole dicarboxylate ester TACN chelators for ^{64}Cu PET imaging in Alzheimer's disease†

Yujue Wang,^a Truc T. Huynh,^{b,c} Nilantha Bandara,^{id} ^b Hong-Jun Cho,^a Buck E. Rogers^b and Liviu M. Mirica^{id} ^{*a,d}

Herein we report a new series of bifunctional chelators (BFCs) with high affinity for amyloid β aggregates, strong binding affinity towards Cu(II), and favorable lipophilicity for potential blood–brain barrier (BBB) penetration. The alkyl carboxylate ester pendant arms show high binding affinity towards Cu(II). The BFCs form stable ^{64}Cu -radiolabeled complexes and exhibit favorable partition coefficient ($\log D$) values of 0.75–0.95. Among the five compounds tested, ^{64}Cu -YW-1 and ^{64}Cu -YW-13 complexes exhibit significant staining of amyloid plaques in *ex vivo* autoradiography studies.

Received 18th August 2021,
Accepted 10th December 2021

DOI: 10.1039/d1dt02767k

rsc.li/dalton

Introduction

According to the Alzheimer's Association, Alzheimer's disease (AD) is the 6th leading cause of death in the United States and the most common cause of dementia worldwide.¹ AD is a neurodegenerative disease; as the disease progresses, symptoms including memory loss, synaptic dysfunction, and decline in learning and thinking abilities are experienced.^{2–4} As the disease progresses, amyloid plaques formed by abnormal aggregation of amyloid β ($\text{A}\beta$) gradually build up in the brains of AD patients, causing brain damage and neuron death. $\text{A}\beta$ peptides are derived from the amyloid precursor protein (APP), and sequential cleavages of APP by β - and γ -secretases generate $\text{A}\beta$ monomers with 39 to 43 amino acid residues in length. The two major isoforms of $\text{A}\beta$ peptides are 40 and 42 amino acids long, named $\text{A}\beta_{40}$ and $\text{A}\beta_{42}$, respectively.^{5–9}

AD is currently incurable, and definitive diagnosis relies heavily on post-modern examination of the brains of patients.^{10–13} As researchers move to target the early stage of AD, determining the presence of amyloid deposits to confirm diagnosis becomes more and more important. Molecular imaging techniques, such as positron emission tomography

(PET), have enabled non-invasive assessment of $\text{A}\beta$ burden in the brains of patients.^{14,15} PET imaging utilizes radiotracers containing positron-emitting radionuclides, such as ^{11}C ($t_{1/2} = 20.4$ min) and ^{18}F ($t_{1/2} = 109.7$ min), which have been extensively studied in the last three decades. ^{11}C radiolabeled Pittsburgh compound-B (^{11}C -PiB) is widely used for imaging fibrillar amyloid species by PET scanning.^{16,17} Three ^{18}F -labelled $\text{A}\beta$ tracers, the benzothiazole derivative ^{18}F -flutemetamol (Vizamyl), and the stilbene derivatives ^{18}F -florbetaben (Neuraceq) and ^{18}F -florbetapir (Amyvid), have been approved by the US Food and Drug Administration (FDA) for estimating $\text{A}\beta$ plaque burdens in patients with cognitive impairment.^{18–22}

However, in clinical usage, both ^{11}C and ^{18}F radiotracers suffer from relatively short half-lives. In addition, these radioisotopes are covalently installed into the target molecules, requiring special synthetic approaches and equipment.²³ Therefore, long-lived radiometals, notably copper-64 ($t_{1/2} = 12.7$ h, $\beta^+ = 17.8\%$; $\beta^- = 38.4\%$), have gained considerable interest in PET imaging.²⁴ Compared with ^{11}C and ^{18}F , the long half-life of ^{64}Cu allows for accumulation in the targeted region and broader clinical applications, especially for use in areas without access to on-site cyclotrons.^{25–27} Moreover, ^{64}Cu could be easily incorporated into target bio-active agents *via* rapid chelation. The common oxidation state of ^{64}Cu in aqueous solution is $^{64}\text{Cu}(\text{II})$, and its d^9 electronic configuration enables the formation of many coordination forms, varying from four-coordinate to six-coordinate using metal chelators containing nitrogen donors, anionic oxygen, or sulfur donors.²⁴

We have recently reported the development of bifunctional chelators (BFCs), which contain an $\text{A}\beta$ -binding motif (2-phenylbenzothiazole derivative) and strong Cu(II)-chelating macro-

^aDepartment of Chemistry, University of Illinois at Urbana-Champaign, 600 S. Mathews Avenue, Urbana, Illinois 61801, USA. E-mail: mirica@illinois.edu

^bDepartment of Radiation Oncology, Washington University School of Medicine, St. Louis, Missouri 63108, USA

^cDepartment of Chemistry, Washington University, St. Louis, Missouri 63130, USA

^dHope Center for Neurological Disorders, Washington University School of Medicine, St. Louis, MO 63110, USA

† Electronic supplementary information (ESI) available: Spectrophotometric titrations, Job's plots, UV–Vis and fluorescence spectra, and the HPLC chromatograms of radiolabeling assays. See DOI: 10.1039/d1dt02767k

cyclic ligands, such as 1,4-dimethyl-1,4,7-triazacyclononane (TACN) and 2,11-diaza[3.3](2,6)pyridinophane (N4) macrocycles.^{28–30} These BFCs exhibit high affinities for A β aggregates and Cu(II) ions and could be used as ⁶⁴Cu amyloid PET imaging agents. The 2-phenylbenzothiazole derivative has shown appreciable A β -binding and fluorescence properties, therefore we continue to take advantage of this molecule as the amyloid binding motif and carry out the modification on the metal chelating fragment, by attaching two ester carboxylate pendant arms to the TACN backbone (Fig. 1), in order to increase the lipophilicity of the bifunctional chelators (BFCs). Our purpose is to design diester-based ⁶⁴Cu PET imaging agents with favorable metal chelating ability and lipophilicity for *in vivo* amyloid PET imaging applications.

Results and discussion

Design and synthesis of BFCs

The bifunctional chelators (BFCs) discussed herein are created by linking the A β -binding fragment 2-(4-hydroxyphenyl)-benzothiazole and the metal-chelating TACN ligand *via* the Mannich reaction (Scheme 1). The amyloid targeting motif was generated by the condensation of 2-aminothiophenol with vanillin, followed by oxidation with atmospheric oxygen (Scheme S1†). To further enhance the metal chelation ability of BFCs, two pendant carboxylate arms were added to the TACN backbone.

Initially, the synthesis of the final products was conducted using established procedures to generate bi-substituted TACN ligands,³¹ followed by the Mannich reaction with 2-(4-OH-phenyl)-benzothiazole and paraformaldehyde (Scheme S2†). However, due to the lack of fluorescence emission for these precursors, we failed to detect the unreacted TACN ligands by either TLC or HPLC, and therefore were unable to separate the impurities from the products. Moreover, the heating conditions could lead to the decomposition of the ester products. Therefore, we developed a new pathway (Scheme 1) by synthesizing **YW-12** as the ligand precursor and then reacting **YW-12** with a series of alkyl-bromoacetates in the presence of a base, generating the final products **YW-1** to **YW-5** that contain *tert*-

butyl, iso-propyl, ethyl, and methyl ester groups, respectively. Hydrolysis of **YW-1** in the presence of concentrated hydrochloric acid generates **YW-13**.

UV-vis absorption spectra were acquired to determine the maximum absorbance wavelength (λ_{abs}) of the ligands and their Cu(II) complexes in PBS (pH = 7.4) buffer (Fig. 2). Based on the UV-vis absorbance spectra, excitation wavelengths (λ_{ex}) of 345–348 nm for BFCs and similar wavelengths for Cu(II) complexes were used to examine their fluorescence properties (Fig. 3). Due to the quenching effect by chelation with Cu(II), the fluorescence intensities of ester BFCs decrease by 3–4 fold, while that of **YW-13** decreases by 8 fold.

Stability constants with metal ions by pH-spectrophotometric titration

Since all ligands contain several acidic and basic functional groups, their acidity constants ($\text{p}K_{\text{a}}$) were determined by UV-vis spectrophotometric titrations. In order to further investigate the metal chelation ability and to quantify it, we performed spectrophotometric titrations of ligands in the presence of Cu(II) ions.

For **YW-1**, UV-vis titrations from pH 3.0 to 11.0 reveal several changes in the spectra, such as the disappearance of the band at 325 nm and the increase of the band at 351 nm with the isosbestic point at 340 nm (Fig. 4). The best fit to the data was obtained with four $\text{p}K_{\text{a}}$ values: 3.30(6), 5.75(5), 8.16(5) and 11.77(3) (Table 1). On the basis of previously reported acidity constants for phenols and amines,^{32,33} we assigned the three lower $\text{p}K_{\text{a}}$ values to the deprotonation of the amine groups on the TACN backbone, and the highest $\text{p}K_{\text{a}}$ value to the phenol deprotonation in the ligand. The other ester containing ligands in the series show similar values to those obtained for **YW-1** (Table 1).

Similar spectrophotometric titrations were performed to determine the stability constants and solution speciation of the Cu(II)-BFC complexes. The $\text{p}K_{\text{a}}$ values of the ligands and the deprotonation of metal-bound water molecules were included in the calculations. The stoichiometry of the Cu(II)-BFC complexes in solution was determined by Job's plot analysis. The plot of **Cu-YW-13** shows a break around 0.5 Cu mole

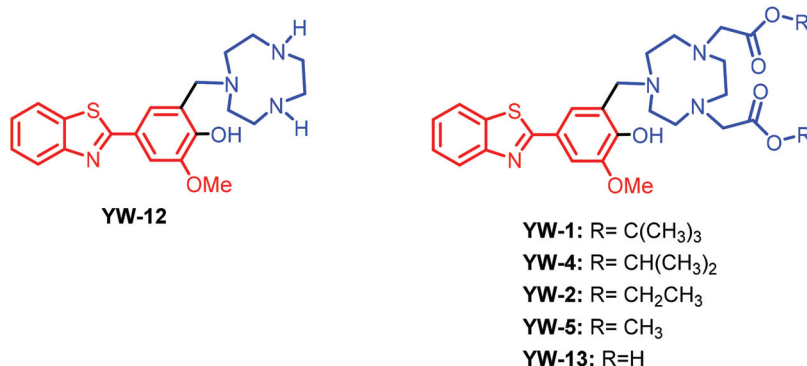
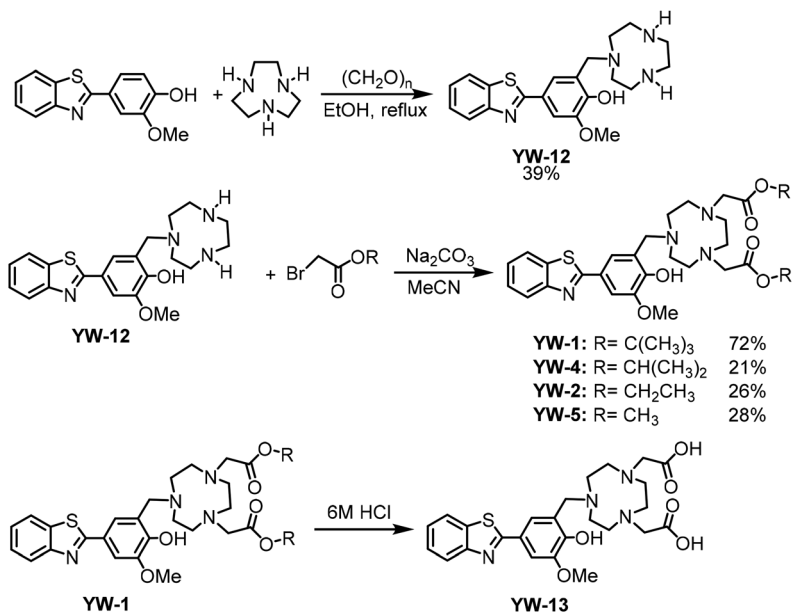


Fig. 1 Structures of the ligands investigated herein. The metal binding and A β -interacting fragments are shown in blue and red, respectively.



Scheme 1 Synthesis of BFCs.

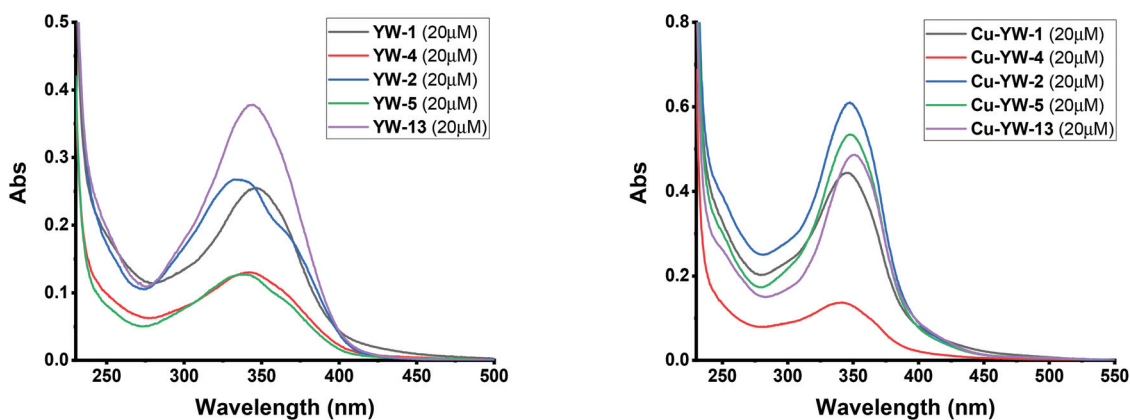


Fig. 2 UV-vis spectra of (left) YW-1 to YW-13 and (right) their Cu(II) complexes in PBS.

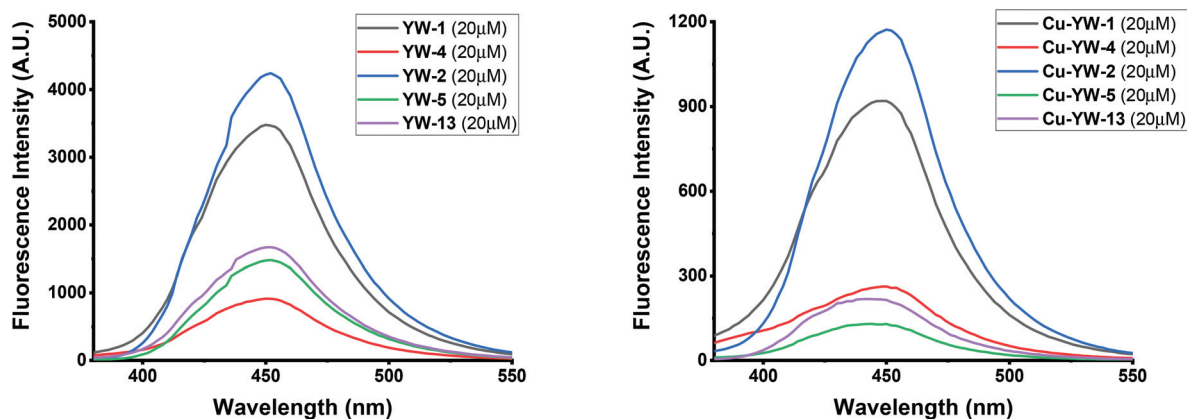


Fig. 3 Emission spectra of (left) YW-1 to YW-13 and (right) their Cu(II) complexes in PBS.

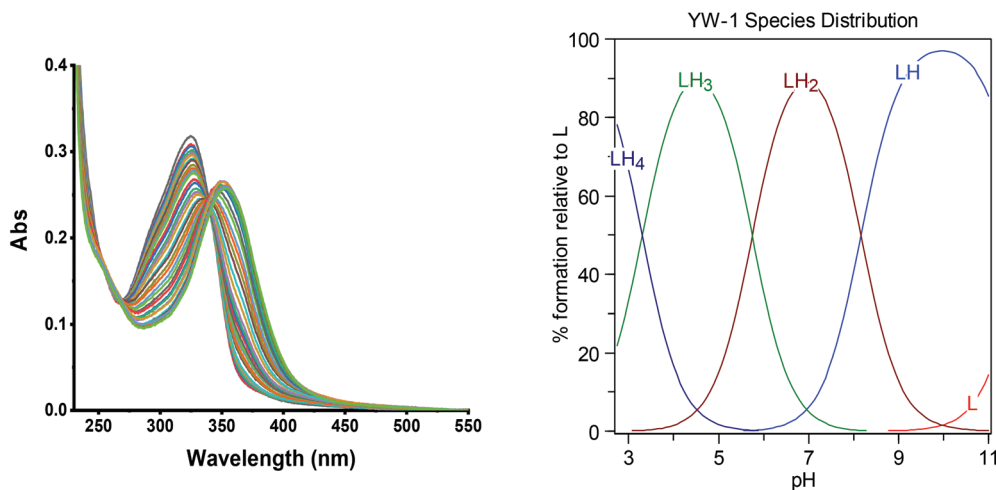


Fig. 4 Variable pH (pH 3–11) UV-vis spectra of YW-1 ([L] = 20 μ M, 25 $^{\circ}$ C, I = 0.1 M NaCl) and the species distribution plot.

Table 1 Acidity constants (pK_a s) of YW-1 to YW-13 determined by spectrophotometric titrations (errors are for the last digit)

Reaction	YW-1	YW-4	YW-2	YW-5	YW-13
$[H_4L]^{3+} = [H_3L]^{2+} + H^+$ (pK_{a1})	3.30(6)	5.09(2)	4.78(3)	4.21(5)	3.83(5)
$[H_3L]^{2+} = [H_2L]^+ + H^+$ (pK_{a2})	5.75(5)	6.48(1)	7.41(2)	6.90(2)	6.44(3)
$[H_2L]^+ = [HL] + H^+$ (pK_{a3})	8.16(5)	8.27(1)	9.42(2)	12.82(1)	7.92(1)
$[HL] = [L]^- + H^+$ (pK_{a4})	11.77(3)	11.98(1)	11.36(1)	11.30(4)	11.84(1)

Table 2 Stability constants ($\log K$) of the Cu(II) complexes of YW-1 to YW-13

Reaction	YW-1	YW-4	YW-2	YW-5	YW-13
$M^{2+} + HL = [MHL]^{2+}$	5.61(13)	6.62(3)	6.89(9)	6.01(2)	3.89(3)
$M^{2+} + L^{-1} = [ML]^+$	23.41(9)	23.27(2)	22.79(7)	22.36(1)	25.56(6)
$[ML(H_2O)]^+ = [ML(OH)] + H^+$	15.27(9)	14.98(2)	15.36(8)	13.79(2)	17.70(7)

fraction, suggesting the formation of a 1:1 complex (Fig. S12[†]).^{28–30} The calculated stability constants show that YW-1 has a larger binding constant ($\log K$) with Cu(II) than YW-2, YW-4, and YW-5 (Table 2). In addition, YW-13, which contains two carboxylic groups instead of ester groups, exhibits the highest binding constant ($\log K$) among all compounds, which is 2–3 orders of magnitude larger than those of ester BFCs.

The species distribution plot of Cu-YW-1 was obtained based on the calculated stability constants (Fig. 5), and the concentration of free Cu(II) with YW-1 is negligible above pH 4, as shown in the plot. The concentrations of free Cu(II) ($pM = -\log[M_{\text{unchelated}}]$) at a specific pH value and the total ion concentration can be calculated from the solution speciation diagrams, and the calculated pCu values for YW-1 and YW-13 are 11.3 and 12.4 at pH 7.4, respectively (Table 3), comparable to the value of 10.7 at pH 7.4 for the strong chelating agent DTPA (diethylenetriaminepentaacetic acid), indicating that our BFCs bind strongly to Cu(II) ions.^{32,34,35}

EPR spectra of copper complexes

To further characterize the Cu(II)–BFC complexes, their X-band CW EPR spectra were recorded in frozen glasses at 77 K. The Cu(II) complexes were prepared right before the EPR experiment by reacting the ligand with 0.8 equivalents of Cu(ClO_4)₂·6H₂O. The EPR spectrum of Cu-YW-1 in a 1:3 (v:v) MeCN:PrCN glass solution reveals a pseudoaxial EPR pattern with three different g values: $g_z = 2.258$, A_z (Cu) = 159 G, $g_y = 2.060$, and $g_x = 2.045$ (Fig. 6). The EPR spectra of Cu-YW-4 and Cu-YW-5 were also obtained in the same way and they show a similar EPR pattern to Cu-YW-1 with $g_z = 2.255$, A_z (Cu) = 165 G, $g_y = 2.055$, $g_x = 2.048$, and $g_z = 2.262$, A_z (Cu) = 165 G, $g_y = 2.041$, $g_x = 2.067$, respectively (Fig. 7 and 8). Overall, these EPR spectra are similar to the ones reported previously for related 2-(4-hydroxyphenyl)benzothiazole TACN derivatives^{28–30} and support the formation of mononuclear Cu complexes in solution.

In general, the R parameter [$R = (g_y - g_z)/(g_x - g_y)$ with $g_x > g_y > g_z$] can be indicative of the predominance of the d_{z^2} or

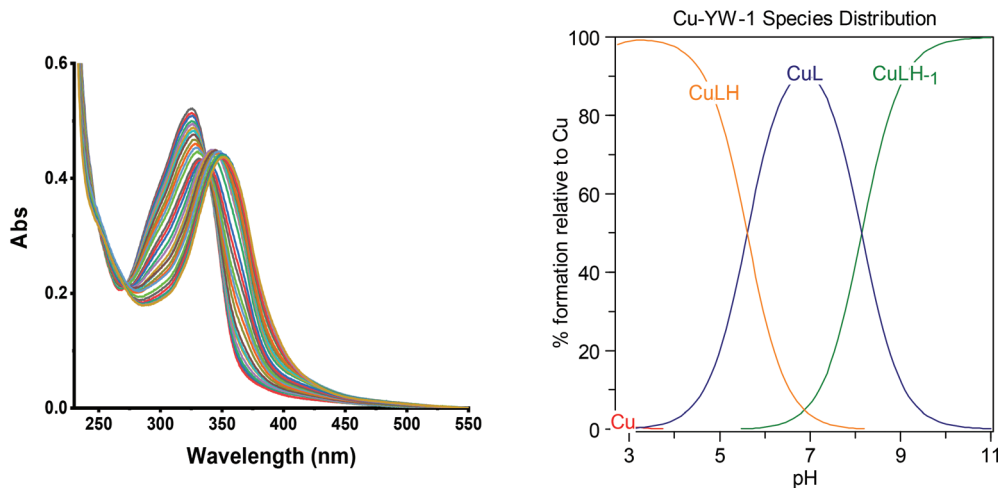


Fig. 5 Variable pH (pH 3–11) UV-vis spectra of the YW-1 and Cu(II) system ($[L] = [Cu^{2+}] = 20 \mu M$, $25^\circ C$, $I = 0.1 M$ NaCl) and the species distribution plot.

Table 3 Calculated pM ($-\log[M]_{free}$; $M = Cu^{2+}$) values for a solution containing a 1 : 1 metal/ligand mixture ($[M^{2+}]_{tot} = [Ligand]_{tot} = 50 \mu M$)

	YW1	YW4	YW2	YW5	YW13	DTPA ^a
pH 6.6	10.5	10.3	9.6	9.4	11.5	9.7
pH 7.4	11.3	11.1	10.6	10.3	12.4	10.7

^a Diethylenetriaminepentaacetic acid (DTPA).³⁴

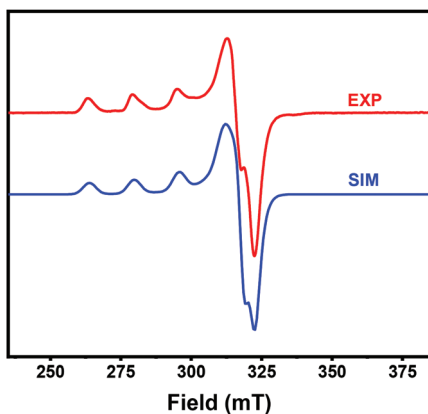


Fig. 6 Experimental and simulated EPR spectra of the Cu-YW-1 complex in 1 : 3 MeCN : PrCN glass at 77 K. The following parameters were used for the simulation: $g_z = 2.258$, A_z (Cu) = 159 G, $g_y = 2.060$, and $g_x = 2.045$.

$d_{x^2-y^2}$ orbital in the ground state of the unpaired electron of the Cu^{2+} ion. When $R > 1$, the greater contribution to the ground state arises from the d_{z^2} orbital, while when $R < 1$, the greater contribution to the ground state comes from the $d_{x^2-y^2}$ orbital. The R value of 0.076 determined for Cu-YW-1 is indicative of a predominantly $d_{x^2-y^2}$ ground state, which is characteristic of Cu(II) complexes with slightly rhombic symmetry and

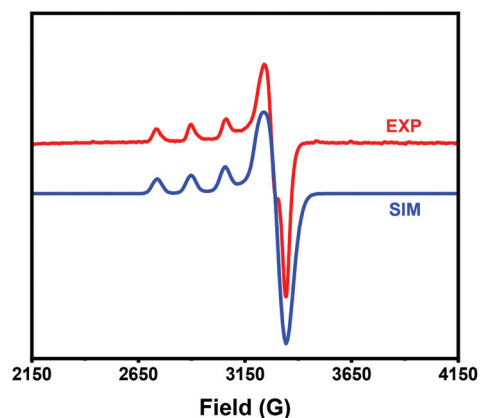


Fig. 7 Experimental and simulated EPR spectra of the Cu-YW-4 complex in 1 : 3 MeCN/PrCN glass at 77 K. The following parameters were used for the simulations: $g_z = 2.255$, A_z (Cu) = 165 G, $g_y = 2.055$, $g_x = 2.048$.

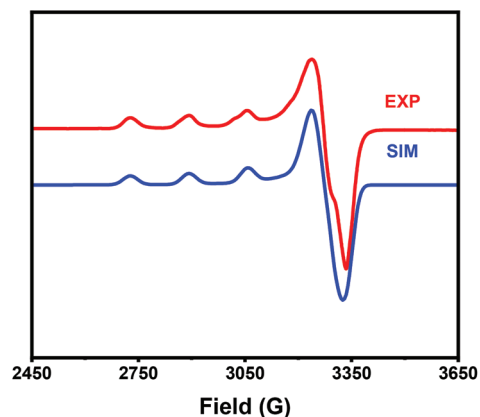


Fig. 8 Experimental and simulated EPR spectra of the Cu-YW-5 complex in 1 : 3 MeCN/PrCN glass at 77 K. The following parameters were used for the simulations: $g_z = 2.262$, A_z (Cu) = 165 G, $g_y = 2.041$, $g_x = 2.067$.

elongation of the axial bonds. **Cu-YW-4** has a similar symmetry with an R value of 0.035.^{36–38}

Interaction of YW-13 with A β ₄₂ fibrils

BFCs investigated herein contain fragments derived from benzothiazole and *o*-vanillin, which bind tightly to A β species, while also exhibiting fluorescence emission that increases in the presence of amyloid fibrils.^{32,39} When a solution of A β ₄₂ fibrils was titrated with **YW-13** and the emission intensity increase was corrected for the intrinsic fluorescence of **YW-13**, a saturation behavior is observed that is best fit with a one-site binding model to give $K_d = 121 \pm 44$ nM (Fig. 9), indicating that this BFC can bind tightly to A β ₄₂ species. We have also attempted to obtain K_d values for the ester BFCs or their Cu complexes, as performed previously,^{28–30} yet the fluorescence intensities were low and negligible increases in intensity were observed upon increasing the concentration of BFCs or their Cu complexes.

Fluorescence imaging of amyloid plaques in 5xFAD mouse brain sections

Ex vivo mouse brain section staining was performed to evaluate each BFC's affinity toward A β species. Brain sections were collected from 11-month-old 5xFAD transgenic mice, which overexpress the mutant form of APP that can be cleaved by β - and γ -secretases to form A β peptides, and develop severe amyloid pathology found in AD.^{40,41} An appreciable amount of fluorescence staining was observed upon incubation of the brain sections for 30 min with 50 μ M solutions of BFCs, especially for **YW-4** and **YW-5** (Fig. 10, left panels). The specific staining of amyloid plaques was confirmed by staining with Congo Red, another amyloid-binding fluorescent dye (Fig. 10, middle panels).^{42,43} The labeling ability of Cu(II) complexes was also probed using mouse brain sections of the same age. Compared to BFCs **YW-4** and **YW-5**, the colocalization of their Cu(II) complex signal with the Congo Red signal is improved, as indicated by Pearson's coefficients. The other BFCs and their Cu(II) complexes also show moderate staining of amyloid aggregates (Fig. S1 and S2†). Overall, these *ex vivo* amyloid

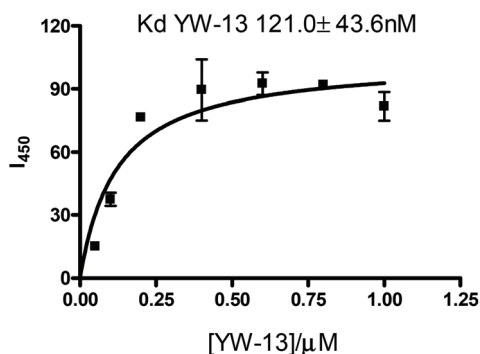


Fig. 9 Direct binding constant measurements of **YW-13** with A β ₄₂ fibrils.

Ligand	Conc. (μ M)	Ligand to Congo Red ratio
YW-4	50	25:1
Cu-YW-4	50	25:1
YW-5	50	25:1
Cu-YW-5	50	25:1

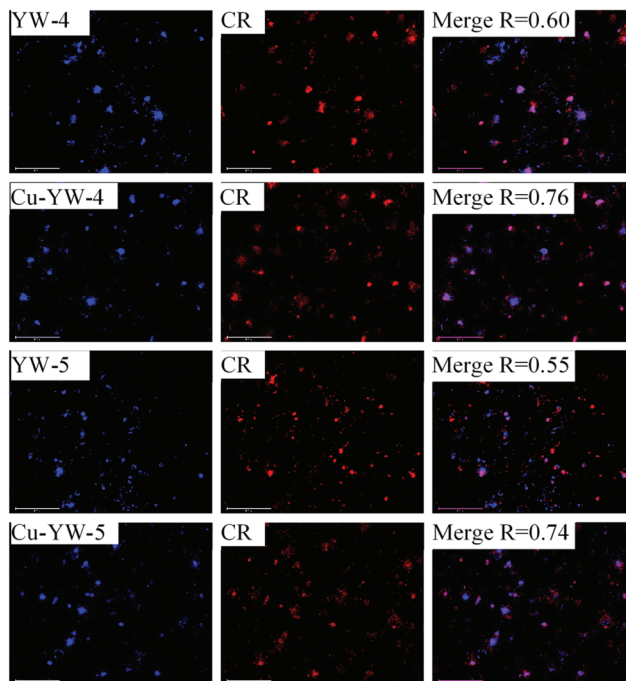


Fig. 10 Fluorescence microscopy images of 5xFAD brain sections incubated with compounds **YW-4** and **YW-5**, their Cu(II) complexes (left panels), Congo Red (middle panels), and merged images (right panels). Magnification: 20 \times . Scale bar: 125 μ m.

binding studies suggest that these BFCs could bind to A β species (see below).

The amyloid binding affinity of the BFCs was further investigated with the AF594-conjugated HJ3.4 antibody (AF594-HJ3.4) that binds to a wide range of A β species.^{30,44–48} Using 6-month-old 5xFAD mouse brain sections, the intense signal of fluorescence staining was observed with the treatment of 50 μ M BFCs or the corresponding Cu(II) complex solutions for 1 h. With less bulky substituents (from the *tert*-butyl group to the methyl group and the hydrogen atom), there is an improvement of the colocalization between BFCs' signal and antibody's signal, as indicated by the calculated Pearson's coefficients (Fig. 11). The specific staining of **Cu-YW-13** is further examined with the 40 \times lens of the fluorescence microscope (Fig. S3†), and it exhibits strong colocalization with the antibody stained regions.

Radiolabeling and log D value determination

The radiolabeling of compounds **YW-1** to **YW-13** was performed using ⁶⁴CuCl₂ and employing the conditions described in the Experimental section.⁴⁹ Quality control assays were con-

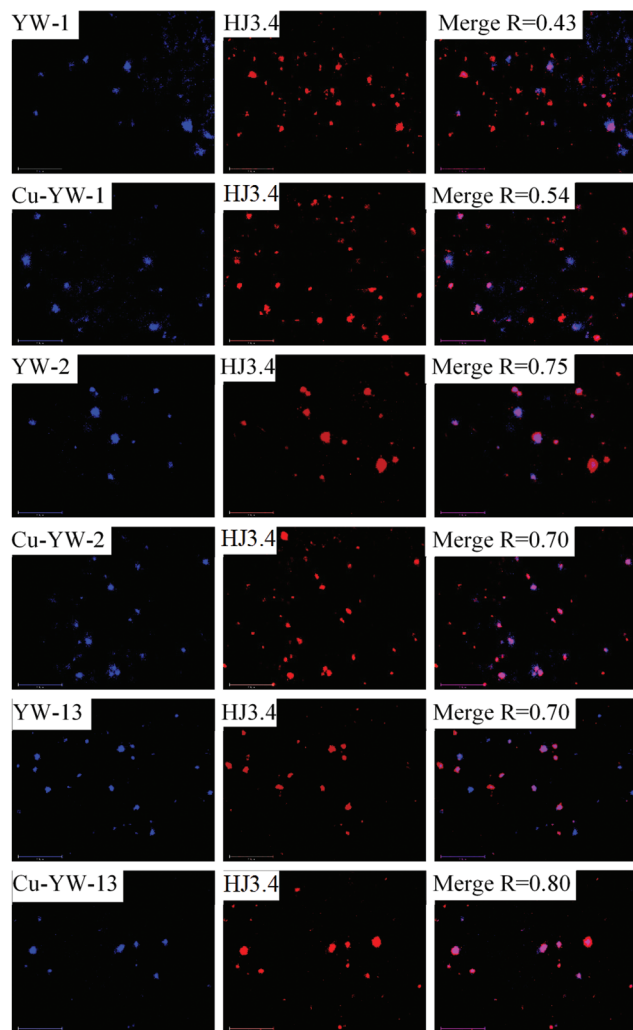


Fig. 11 Fluorescence microscopy images of 5xFAD brain sections incubated with compounds YW-1, YW-2, and YW-13, their Cu(II) complexes (left panels), the AF594-HJ3.4 antibody (middle panels), and merged images (right panels). Concentrations used: [BFC] = [Cu²⁺] = 50 μ M, [HJ3.4] = 1 μ g ml⁻¹. Magnification: 20x. Scale bar: 125 μ m.

ducted using HPLC and/or TLC. All radiochemical yields were >95% within minutes at 45 °C, with specific activities of 100 Ci per mmol or greater. Therefore, all radiolabeled complexes were used directly without further purification.

For compounds to be used in neuroimaging applications, one critical factor is the penetration of the blood brain barrier (BBB). Although the Lipinski's rules could offer insights for designing molecules with favorable lipophilicity, it is necessary to obtain experimental results for the evaluation of the BBB permeability.⁵⁰ To determine the hydrophobicity of the radiolabeled compounds, the octanol/water partition coefficient values $\log D$ were determined for the ⁶⁴Cu complexes of YW-1 to YW-13 (Table 4). Gratifyingly, the obtained $\log D$ values for the ⁶⁴Cu-radiolabeled complexes YW-1 to YW-5 are in the range of 0.72–0.95, which suggest their potential ability to cross the BBB. By comparison, the ⁶⁴Cu complex of YW-13,

Table 4 Molecular weights (MWs) of ligands YW-1 to YW-13, and measured $\log D$ values for the corresponding ⁶⁴Cu-radiolabeled complexes

Ligand	MWs of ligands (g·mol ⁻¹)	$\log D$ (⁶⁴ Cu complexes)
YW-1	626.8	0.95 ± 0.07
YW-4	598.3	0.91 ± 0.07
YW-2	570.7	0.90 ± 0.03
YW-5	542.7	0.72 ± 0.02
YW-13	514.6	-0.68 ± 0.10

which does not contain the ester group on the acetate branch, exhibits a negative $\log D$ value of -0.68 ± 0.10 and thus is not expected to cross the BBB. The radio-HPLC profiles suggested that YW-13 chelates tightly with ⁶⁴Cu, while ⁶⁴Cu-YW-2 could undergo decomposition in the aqueous media, due to the potential hydrolysis of the ester groups (Fig. S14†).

Autoradiography studies

Ex vivo autoradiography studies using the 6 brain sections of 11-month-old 5xFAD and age-matched WT mice were conducted to determine the specific binding of the ⁶⁴Cu-labeled

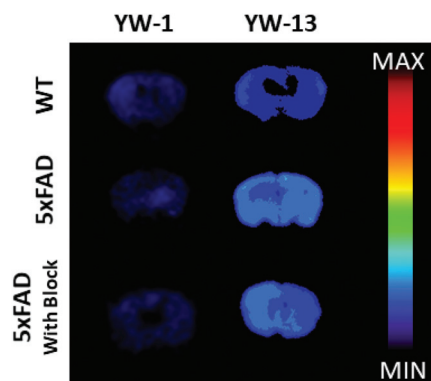


Fig. 12 Autoradiography images of the brain sections of WT and 5xFAD mice, in the absence and presence of a known A β specific blocking agent.

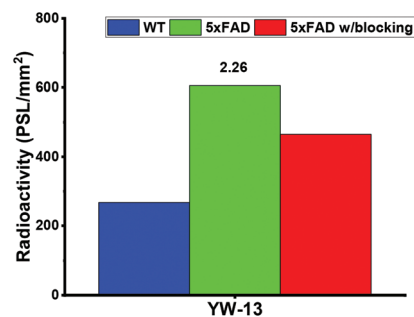


Fig. 13 Average radioactivity of the brain sections in the autoradiography images. The numbers in the bar graph are the intensity ratios of 5xFAD to WT in each group.

BFCs to the amyloid plaques. The brain sections were stained, washed, and imaged as described in the Experimental section.⁴⁹ Unfortunately, ⁶⁴Cu-YW-1 exhibits very low radioactivity intensity when staining the 5xFAD mouse brain sections (Fig. 12, left column). Upon treatment with ⁶⁴Cu-YW-13 (Fig. 12, right column), we observed an increased autoradiography intensity and ⁶⁴Cu-YW-13 exhibits a 2.26 intensity ratio of 5xFAD to WT staining (Fig. 13). The specific binding of the radiolabeled BFCs to amyloid plaques was further confirmed by blocking the brain sections with the non-radioactive blocking agent (**B**₁, Fig. S15†).

Conclusions

To summarize, we have designed and synthesized five BFCs YW-1 to YW-13 containing a 2-(4-hydroxyphenyl)benzothiazole fragment as the amyloid targeting motif and triazacyclononane-dicarboxylate ester metal chelator. Modification of the synthetic pathway allows for the generation of a series of BFCs in a direct approach. The evaluation of the A β -binding affinity for these BFCs and their ⁶⁴Cu complexes was probed by *ex vivo* AD mouse brain section fluorescence imaging and autoradiography studies. These results show that the Cu(II) complexes of the dicarboxylic acid YW-13 bind more selectively to the amyloid plaques than the Cu(II) complexes of the dicarboxylate esters YW-1 to YW-5. The ⁶⁴Cu-radiolabeled dicarboxylate ester BFCs exhibit moderate log*D* values around 0.9, suggesting that they should be BBB permeable. Unfortunately, the ⁶⁴Cu complex of YW-13, which has favorable amyloid binding affinity and metal chelating ability, exhibits a negative log*D* value.

Overall, the resulting BFCs could be readily radiolabeled with ⁶⁴Cu for PET imaging purposes. More efforts need to be devoted for improving the lipophilicity of such BFCs for *in vivo* applications. These results further suggest that the presence of two carboxylic acid groups appended to the TACN macrocycle makes the corresponding chelators hydrophilic for BBB permeability, and the related systems containing only one carboxylic acid or ester group should be more appropriate for *in vivo* applications.⁵¹

Conflicts of interest

The authors declare no competing financial interest.

Acknowledgements

This work was supported by research funding from the NIH (R01GM114588 to L. M. M.). We thank the small animal imaging facilities at Washington University School of Medicine for excellent technical assistance and the Isotope Production Group at Washington University for the production of ⁶⁴Cu.

References

- 2020 Facts and Figures Report – Alzheimer's Association, *Alzheimer's Dementia*, 2020, **16**, 391–460.
- C. Duyckaerts, B. Delatour and M. C. Potier, *Acta Neuropathol.*, 2009, **118**, 5–36.
- C. R. Jack Jr., D. A. Bennett, K. Blennow, M. C. Carrillo, B. Dunn, S. B. Haeberlein, D. M. Holtzman, W. Jagust, F. Jessen, J. Karlawish, E. Liu, J. L. Molinuevo, T. Montine, C. Phelps, K. P. Rankin, C. C. Rowe, P. Scheltens, E. Siemers, H. M. Snyder, R. Sperling and Contributors, *Alzheimer's Dementia*, 2018, **14**, 535–562.
- R. Mayeux and Y. Stern, *Cold Spring Harbor Perspect. Med.*, 2012, **2**, a006239.
- J. K. Kasim, I. Kavianinia, P. W. R. Harris and M. A. Brimble, *Front. Chem.*, 2019, **7**, 472.
- G. Thinakaran and E. H. Koo, *J. Biol. Chem.*, 2008, **283**, 29615–29619.
- G. F. Chen, T. H. Xu, Y. Yan, Y. R. Zhou, Y. Jiang, K. Melcher and H. E. Xu, *Acta Pharmacol. Sin.*, 2017, **38**, 1205–1235.
- Y. W. Zhang, R. Thompson, H. Zhang and H. Xu, *Mol. Brain*, 2011, **4**, 3.
- K. Pauwels, T. L. Williams, K. L. Morris, W. Jonckheere, A. Vandersteen, G. Kelly, J. Schymkowitz, F. Rousseau, A. Pastore, L. C. Serpell and K. Broersen, *J. Biol. Chem.*, 2012, **287**, 5650–5660.
- J. L. Cummings, T. Morstorf and K. Zhong, *Alzheimers Res. Ther.*, 2014, **6**, 37.
- J. Cummings, G. Lee, A. Ritter, M. Sabbagh and K. Zhong, *Alzheimer's Dementia*, 2020, **6**, e12050.
- J. Hardy and D. Allsop, *Trends Pharmacol. Sci.*, 1991, **12**, 383–388.
- P. G. Vallet, R. Guntern, P. R. Hof, J. Golaz, A. Delacourte, N. K. Robakis and C. Bouras, *Acta Neuropathol.*, 1992, **83**, 170–178.
- S. M. Ametamey, M. Honer and P. A. Schubiger, *Chem. Rev.*, 2008, **108**, 1501–1516.
- J. Czernin and M. E. Phelps, *Annu. Rev. Med.*, 2002, **53**, 89–112.
- W. E. Klunk, H. Engler, A. Nordberg, Y. Wang, G. Blomqvist, D. P. Holt, M. Bergström, I. Savitcheva, G.-F. Huang, S. Estrada, B. Ausén, M. L. Debnath, J. Barletta, J. C. Price, J. Sandell, B. J. Lopresti, A. Wall, P. Koivisto, G. Antoni, C. A. Mathis and B. Långström, *Ann. Neurol.*, 2004, **55**, 306–319.
- K. S. Frederiksen, S. G. Hasselbalch, A. M. Hejl, I. Law, L. Hojgaard and G. Waldemar, *Dement. Geriatr. Cogn. Disord. Extra*, 2012, **2**, 610–621.
- K. Serdons, C. Terwinghe, P. Vermaelen, K. Van Laere, H. Kung, L. Mortelmans, G. Bormans and A. Verbruggen, *J. Med. Chem.*, 2009, **52**, 1428–1437.
- S. R. Choi, G. Golding, Z. Zhuang, W. Zhang, N. Lim, F. Hefti, T. E. Beneditum, M. R. Kilbourn, D. Skovronsky and H. F. Kung, *J. Nucl. Med.*, 2009, **50**, 1887–1894.

- 20 B. C. Uzuegbunam, D. Librizzi and B. H. Yousefi, *Molecules*, 2020, **25**, 977.
- 21 H. F. Kung, S. R. Choi, W. Qu, W. Zhang and D. Skovronsky, *J. Med. Chem.*, 2010, **53**, 933–941.
- 22 K. Herholz and K. Ebmeier, *Lancet Neurol.*, 2011, **10**, 667–670.
- 23 M. Conti and L. Eriksson, *EJNMMI Phys*, 2016, **3**, 8.
- 24 M. Shokeen and C. J. Anderson, *Acc. Chem. Res.*, 2009, **42**, 832–841.
- 25 V. Maheshwari, J. L. J. Dearling, S. T. Treves and A. B. Packard, *Inorg. Chim. Acta*, 2012, **393**, 318–323.
- 26 A. C. Sedgwick, J. T. Brewster, P. Harvey, D. A. Iovan, G. Smith, X.-P. He, H. Tian, J. L. Sessler and T. D. James, *Chem. Soc. Rev.*, 2020, **49**, 2886–2915.
- 27 T. J. Wadas, E. H. Wong, G. R. Weisman and C. J. Anderson, *Curr. Pharm. Des.*, 2007, **13**, 3–16.
- 28 A. K. Sharma, J. W. Schultz, J. T. Prior, N. P. Rath and L. M. Mirica, *Inorg. Chem.*, 2017, **56**, 13801–13814.
- 29 Y. Huang, H.-J. Cho, N. Bandara, L. Sun, D. Tran, B. E. Rogers and L. M. Mirica, *Chem. Sci.*, 2020, **11**, 7789–7799.
- 30 H. J. Cho, T. T. Huynh, B. E. Rogers and L. M. Mirica, *Proc. Natl. Acad. Sci. U. S. A.*, 2020, **117**, 30928–30933.
- 31 H.-S. Chong, X. Sun, Y. Zhong, K. Bober, M. R. Lewis, D. Liu, V. C. Ruthengael, I. Sin and C. S. Kang, *Eur. J. Org. Chem.*, 2014, 1305–1313.
- 32 A. K. Sharma, S. T. Pavlova, J. Kim, D. Finkelstein, N. J. Hawco, N. P. Rath, J. Kim and L. M. Mirica, *J. Am. Chem. Soc.*, 2012, **134**, 6625–6636.
- 33 N. Bandara, A. K. Sharma, S. Krieger, J. W. Schultz, B. H. Han, B. E. Rogers and L. M. Mirica, *J. Am. Chem. Soc.*, 2017, **139**, 12550–12558.
- 34 T. Storr, M. Merkel, G. X. Song-Zhao, L. E. Scott, D. E. Green, M. L. Bowen, K. H. Thompson, B. O. Patrick, H. J. Schugar and C. Orvig, *J. Am. Chem. Soc.*, 2007, **129**, 7453–7463.
- 35 N. Choudhary, M. D. Jaraquemada-Pelaez, K. Zarschler, X. Z. Wang, V. Radchenko, M. Kubeil, H. Stephan and C. Orvig, *Inorg. Chem.*, 2020, **59**, 5728–5741.
- 36 C. V. Esteves, P. Lamosa, R. Delgado, J. Costa, P. Désogère, Y. Rousselin, C. Goze and F. Denat, *Inorg. Chem.*, 2013, **52**, 5138–5153.
- 37 B. J. Hathaway and D. E. Billing, *Coord. Chem. Rev.*, 1970, **5**, 143–207.
- 38 B. J. Hathaway and A. A. G. Tomlinson, *Coord. Chem. Rev.*, 1970, **5**, 1–43.
- 39 M. Necula, R. Kayed, S. Milton and C. G. Glabe, *J. Biol. Chem.*, 2007, **282**, 10311–10324.
- 40 H. Oakley, S. L. Cole, S. Logan, E. Maus, P. Shao, J. Craft, A. Guillozet-Bongaarts, M. Ohno, J. Disterhoft, L. Van Eldik, R. Berry and R. Vassar, *J. Neurosci.*, 2006, **26**, 10129–10140.
- 41 E. Drummond and T. Wisniewski, *Acta Neuropathol.*, 2017, **133**, 155–175.
- 42 W. E. Klunk, J. W. Pettegrew and D. J. Abraham, *J. Histochem. Cytochem.*, 1989, **37**, 1273–1281.
- 43 E. I. Yakupova, L. G. Bobyleva, I. M. Vikhlyantsev and A. G. Bobylev, *Biosci. Rep.*, 2019, **39**, BSR20181415.
- 44 K. E. Schwetye, J. R. Cirrito, T. J. Esparza, C. L. Mac Donald, D. M. Holtzman and D. L. Brody, *Neurobiol. Dis.*, 2010, **40**, 555–564.
- 45 T. J. Esparza, N. C. Wildburger, H. Jiang, M. Gangolli, N. J. Cairns, R. J. Bateman and D. L. Brody, *Sci. Rep.*, 2016, **6**, 38187.
- 46 R. J. Perrin, A. M. Fagan and D. M. Holtzman, *Nature*, 2009, **461**, 916–922.
- 47 A. M. Fagan and D. M. Holtzman, *Biomarkers Med.*, 2010, **4**, 51–63.
- 48 L. Sun, A. K. Sharma, B.-H. Han and L. M. Mirica, *ACS Chem. Neurosci.*, 2020, **11**, 2741–2752.
- 49 See ESI.†
- 50 C. A. Lipinski, F. Lombardo, B. W. Dominy and P. J. Feeney, *Adv. Drug Delivery Rev.*, 2001, **46**, 3–26.
- 51 Y. Wang, T. T. Huynh, H.-J. Cho, Y.-C. Wang, B. E. Rogers and L. M. Mirica, *Inorg. Chem.*, 2021, **60**, 12610–12620.